Cu-based Shape Memory Microwires: Towards Complex Structures

by

Mac Gager

Submitted to the Department of Materials Science and Engineering
in Partial Fulfillment of the Requirements for the Degree of

Bachelor of Science in Materials Science and Engineering
at the
Massachusetts Institute of Technology

June 2014

Signature redacted

Signature of Author.....
Mac Gager
Department of Materials Science and Engineering
May 2, 2014

Signature redacted

Certified by.....
Christopher A. Schuh
Department Head of Materials Science and Engineering
Thesis Supervisor

Signature redacted

Accepted by.....
Jeffrey C. Grossman
Carl Richard Soderberg Associate Professor of Power Engineering
Chair, Undergraduate Committee

Cu-based Shape Memory Microwires:
Towards Complex Structures

by

Mac Gager

Submitted to the Department of Materials Science and Engineering
on May 2 2014 in Partial Fulfillment of the Requirements for
the Degree of Bachelor of Science in Materials Science and Engineering

Abstract

Shape memory alloys are a distinctive type of material that exhibits the fascinating properties of the shape memory effect and superelasticity. Shape memory properties are characterized by the diffusionless phase transformation between austenite and martensite that can be thermally or stress induced. Cu-based shape memory alloys provide an exciting area of research due to lower costs and higher working temperatures compared to Ni-Ti alloys prevalent in industry today. This work investigates the shape memory properties of oligocrystalline Cu-Al-Ni and Cu-Al-Mn-Ni microwires produced using a melt spinner. The melt spinner yielded continuous wires in quantities useful for the creation of complex structures. The composition of the wires is observed to change throughout processing of alloys and wires. Electropolishing rates were determined for improving surface texture and size constraint.

Thesis Supervisor: Christopher A. Schuh

Title: Department Head and Danae and Vasilis Salapatas Professor of Metallurgy

Acknowledgements

First, I would like to thank Nihan Tuncer for her support throughout this entire thesis. I wouldn't have been able to do this without her assistance in fabricating wires and the overall direction she provided. I would also like to thank Chris Schuh, my thesis advisor, for taking me in with the group. Also, many thanks to the rest of the Schuh group members for their assistance, sharing lab space, and teaching me about their own research.

Table of Contents

List of Figures

List of Tables

1. Introduction

Arne Olander first discovered peculiar properties in an Au-Cd alloy in 1932. A material deformed at a cool temperature would return to its original state upon heating [1]. This was the first report of the shape memory effect. Since then shape memory alloys have been explored in many families of alloys including Au-Cd [2], Fe-Mn-Si [3], Ni-Ti [4], Cu-Al-Ni [5], among others. The fundamental theory of shape memory behavior has been studied in depth, although the mechanisms for transformations are not fully understood today. Ni-Ti is the most commercially successful shape memory alloy, with heavy applications in the medicine and aerospace industries [6]. However, Ni-Ti is prohibitively expensive for many applications, thus an alternative is needed. This chapter will describe the fundamental crystallography of shape memory alloys, the thermomechanical properties of the shape memory effect and superelasticity, as well as current work on Ni-Ti and alternative alloys, specifically Cu-based alloys.

1.1 Crystallography

Shape memory alloys are characterized by a diffusionless, solid-to-solid reversible phase transformation between austenite and martensite known as martensitic transformation. Austenite is a high temperature phase, while martensite is the lower temperature phase. Most SMA austenite phases are composed of a super lattice structure with body centered cubic sub lattices while martensite lattices are typically orthorhombic or monoclinic [7]. The austenite phase has higher crystallographic symmetry than martensite, leading to variants of

martensite [7]. When transforming to martensite, different variants may arise; the coexistence of multiple variants of martensite is know as a twin [8]. Austenite transforms to martensite when nucleation and growth of crystals occur, this transformation can be thermally or stress induced under isothermal conditions. Thermally induced phase transformation is related to the shape memory effect, while the stress induced phase transformation is related to superelasticity. Both the shape memory effect and superelasticity are critical properties for applications of shape memory alloys.

1.2 Shape memory effect

The shape memory effect involves the transformation of austenite to martensite, a martensite to martensite transformation, and cycles of heating and cooling. The austenite, twinned martensite, and detwinned martensite lattices are represented schematically in Figure 1.1. The red atoms represent the austenite lattice and the blue atoms represent the martensite lattices. Austenite is stable to the right of the 4 black lines, at high temperatures and low stresses, while martensite is stable to the left of the 4 black lines, at low temperatures and high stresses.

For the shape memory effect, the material is first cooled from austenite to martensite, from right to left along the green arrow in Figure 1.1. The transformations occur over a range of temperatures, beginning at the martensite start temperature (Ms) and ending at the martensite finish temperature (Mf) when the material has fully transformed to martensite. The martensite variants will be

arranged such that there is little or no macroscopic change to the sample. The resulting microstructure is represented in the bottom left corner of Figure 1.1, shown schematically with 2 variants of martensite. The martensite sample is then subjected to deformation and macroscopic change occurs as the variants are rearranged. When the deformation force is removed the deformed macroscopic state is preserved, denoted by the single directionality of the black arrow.

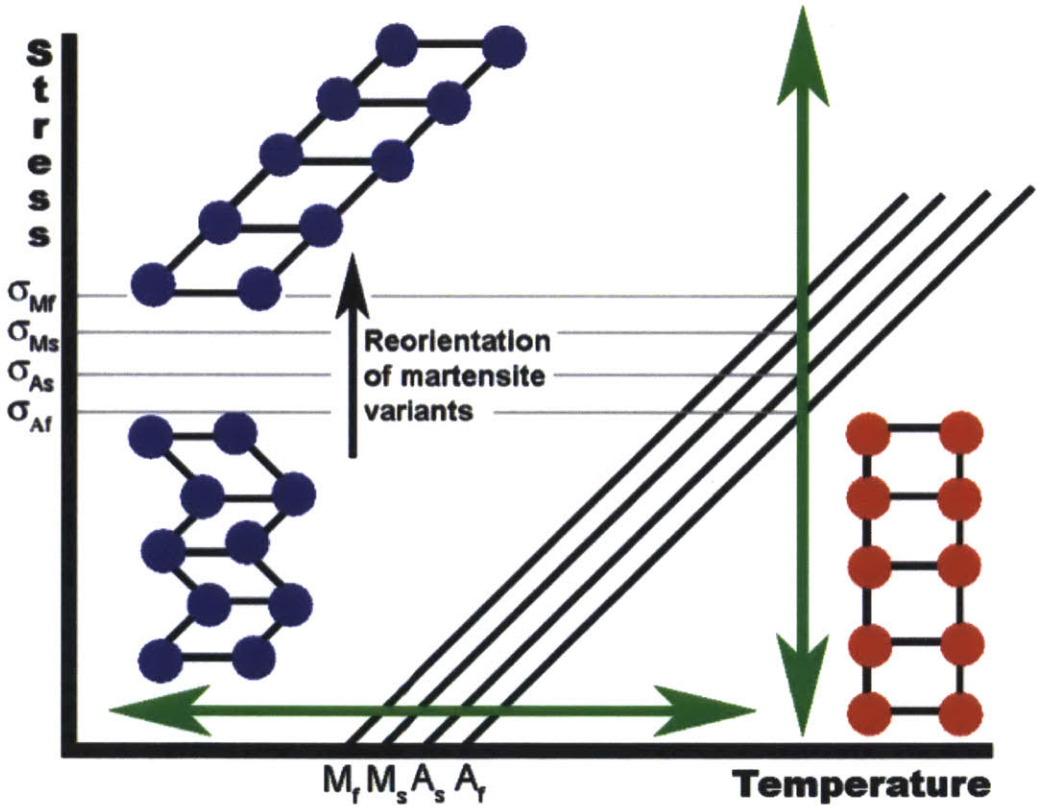

Figure 1.1 Diagram of austenite and martensite transformations in temperature-stress space [9].

The material is now heated to a temperature where austenite is stable. During heating, martensite begins to transform to austenite at the austenite start

temperature (As) and is finished transforming when the material is all austenite after the austenite finish temperature (Af). This atomic, diffusionless transformation cycle is reversible.

The transition temperatures are dependent on sample composition, size, and heat treatment [10]. Hysteresis occurs from cycling the material over the temperature range, as seen in Figure 1.2 (a), leading to dissipation of energy through frictional work.

1.3 Superelasticity

Superelasticity, also known as pseudoelasticity, allows some shape memory alloys to achieve extremely high recoverable strains. Recoverable strains of greater than 10% have been observed in some alloys before plastic deformation occurs [11]. Most metals can only achieve recoverable strains of less than 2%. In this case, the material begins at a temperature slightly above the austenite finish temperature, where austenite is stable. The transformation to martensite is triggered by external stress shown by moving up the vertical green arrow in Figure 1.1, from red austenite to blue martensite, as stress increases. Macroscopic deformation occurs as the material is strained. When the external stresses is removed the material returns to its original form. If the external stress is too high, plastic deformation will occur and not all strain will be recoverable, or the sample could yield.

Similar to the thermally induced transformation, this stress induced transformation occurs over a range of stresses. The forward transformation begins when the martensite start stress, σ_{Ms}, is reached and is completed when the stress

increases further to the martensite finish stress, σ_{Mf}. The reverse transformation occurs as the stress is removed. Austenite begins to form at the austenite start stress, σ_{As}, and the transformation is complete after the austenite finish stress, σ_{Af}, is reached.

Also similar to the thermally induced transformation, the distinct transition stresses lead to hysteresis through stress cycles as seen in Figure 1.2 (b). Energy is lost as heat in order for the transformations to occur.

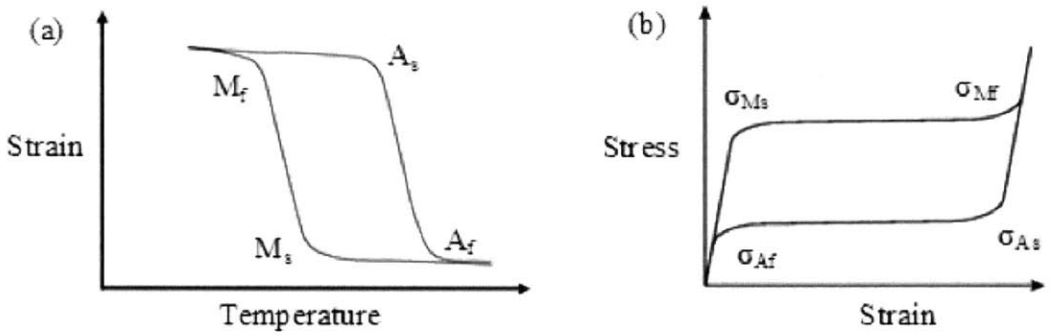

Figure 1.2. (a) Schematic of the shape memory effect hysteresis under constant stress. (b) Schematic of superelastic hysteresis under isothermal conditions. Adapted from [12].

1.4 Current Applications

The most prevalent shape memory alloy used in industry today is Nitinol. Nitinol was discovered accidently by researchers in the Naval Ordnance Laboratory (hence the name) in 1959 [13][14]. Nitinol is a nickel-titanium alloy of roughly equal atomic percentages. The transition temperatures can be controlled to some extent by post processing heat treatment methods, but are typically spread around

30-40 degrees Celsius [15]. Nitinol is highly biocompatible and has found extensive applications in medicine ranging from stents and sutures to orthodontic brackets. Nitinol is also common in eyeglass frames to allow accidental bending without fracture.

Other applications for shape memory alloys include actuators and sensors in a variety of markets. Shape memory alloys are common in MEMS devices as valves and actuators. Ni-Ti-Cu springs are used to control flow of transmission fluids and anti-scalding valves of Ni-Ti-Cu seal hot water flow above scalding temperatures. Thermally activated SMAs are also used as current interrupters to prevent battery meltdowns. [6]

1.5 Cu-based shape memory alloys

A number of Cu-based alloys have been tested for shape memory properties and show promise as an alternative to Nitinol. Cu-based alloys are much less expensive than Ni-Ti in terms of both basic material cost and processing [16]. Interesting and useful properties that Ni-Ti lacks, such as ability to be welded, and high thermal and electronic conductivity are readily available in Cu- based alloys [17]. These characteristics lead to Cu-based alloys being an area of active research, however, the mechanical properties of Ni-Ti remain superior to Cu-based alloys at this time.

1.5.1 Single Crystals, Polycrystals, and Oligocrystals

Shape memory performance for all alloys is heavily dictated by microstructure. For Cu-based alloys, the key aspect of microstructure impacting performance is grain boundaries.

Single crystals of Cu-based alloys have excellent shape memory and superelasticity properties. The absence of grain boundaries makes the transition from austenite to martensite easier and large recoverable strains are achievable. This means a small hysteresis loop with little energy wasted. However, the production of single crystals is more involved and much more expensive than polycrystals, making them unsuitable to replace Nitinol.

The extensive network of grain boundaries found in polycrystals is detrimental to the performance of Cu-based shape memory alloys. The transition from austenite to martensite occurs from the nucleation and growth of martensitic plates triggered by heating or stress. As the material expands during the transition grain boundaries are sources of friction and resist the growth of the martensitic plates. Incompatibilities between grains also inhibit transformation. This results in an additional energy barrier for the transformation. Stress can build up and lead to fracture if the transition stress or temperature becomes too high. Triple junctions (the meeting of three grain boundaries) are very likely to be areas of high stress concentration. Triple junctions can lead to areas of a polycrystal not fully transforming or transforming to a different variant of martensite [9], both are non-ideal for shape memory performance. To mitigate the effects of grain boundaries on performance, the total free surface area to grain boundary ratio must be increased.

One way to do this is through the use of oligocrystals. Oligocrystalline materials have grain boundaries, but they are orientated as bamboo-like grain structures where grain boundaries are perpendicular to the longitudinal axis of the structure as seen in Figure 1.3. This leads to a significant reduction in triple junctions relative to polycrystals. Constraining dimensions to enable grain sizes similar wire diameter can lead to the complete absence of triple junctions. For shape memory alloy microwires, this means stress concentrations are replaced by free surfaces resulting in single crystalline-like performance. [9]

Oligocrystals provide an exciting opportunity where the desirable properties of single crystals (absence of grain boundaries inhibiting performance) are captured, and the expensive production costs can be avoided.

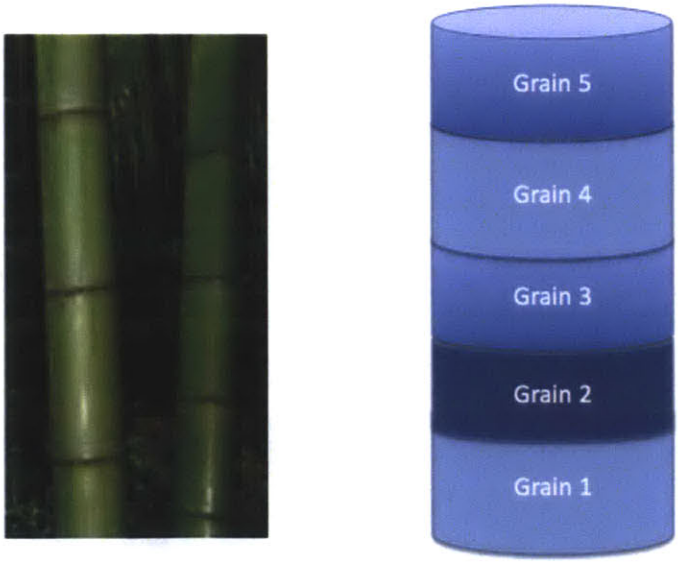

(a) (b)

Figure 1.3. (a) A picture of bamboo showing oligocrystalline like structure [18] and (b) a schematic of grains in an oligocrystalline wire.

1.5.2 Microstructure

The reversible transition from austenite to martensite relies on the proper microstructure. For Cu-Al-Ni, the β-phase is transformed to β' or γ depending on Al composition [19]. A phase diagram of Cu-Al-3wt%Ni, a composition similar to the ones used in this research, is shown in Figure 1.4. The addition of Mn to the system increases the range of Al that allows for shape memory behavior. In order to secure the high temperature β-phase at room temperature, the alloy is heat treated and subsequently water quenched as described in Chapter 2.2.

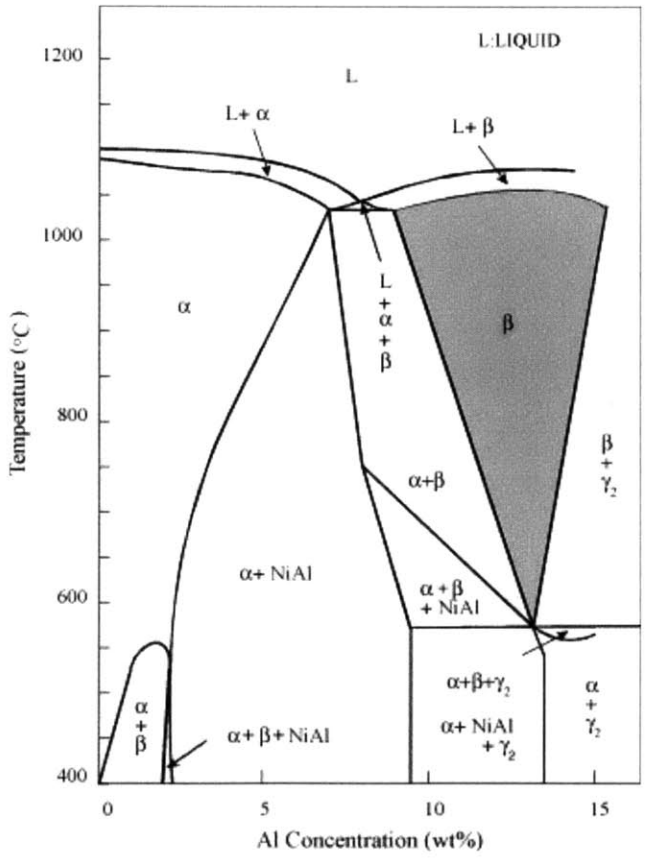

Figure 1.4. Vertical section of the Cu-Al-Ni phase diagram at 3wt%Ni with the β-phase shaded in gray [19].

2. Methodology

2.1 Wire casting

Shape memory alloys were drawn into wires using a wire casting, rapid solidification technique. Alloys of Cu-Al-Mn-Ni and Cu-Al-Ni were drawn. As displayed in Figure 2.1 the wire caster, or melt spinner, consists of a silica crucible containing the alloy that is heated by an induction coil and a rotating drum. The rotating drum is filled with water that is held against the walls by centrifugal forces. The crucible has a small orifice, 100-300um depending on the viscosity of the melt, at the bottom of the tapered end to allow for the alloy to be ejected. The crucible containing the alloy is subjected to low vacuum conditions to prevent oxidation as the temperature is increased.

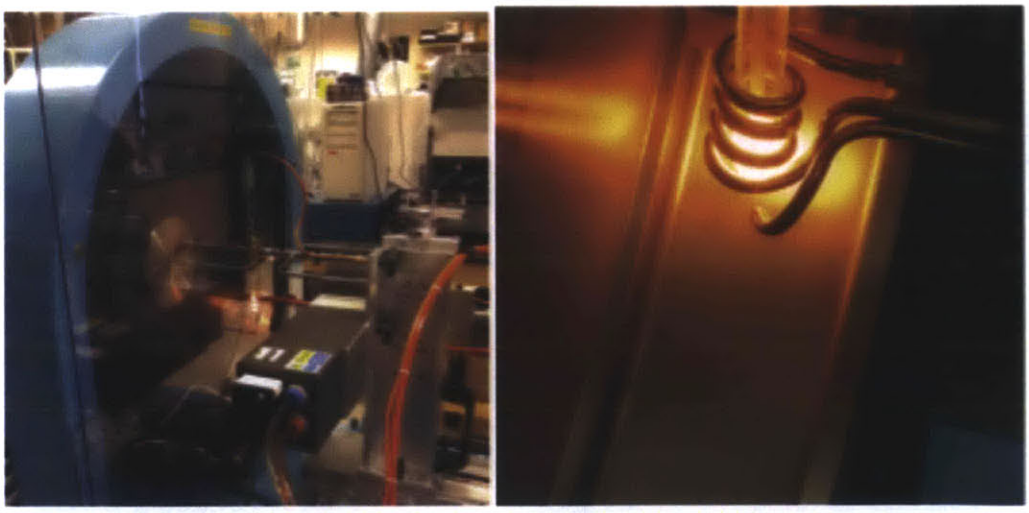

(a) (b)

Figure 2.1. (a) Melt spinner set up used to fabricate microwires and (b) a close up of a glowing alloy being heated by the induction coil [20].

Once the material melts and reaches a critical viscosity, the melt is ejected through the orifice at the tip of the tube via the application of inert gas pressure. A filament of molten alloy is forced out of the orifice and into the water, where it is quenched and rotated away as a microwire. The ejection pressure was 4 bar for all trials and the speed of the drum was 324-330 rpm. Each crucible was filled with approximately 6 grams of alloy in 4-7 pieces.

The characteristics of the resulting microwires are dependent on a number of factors in the wire casting process. The rotation speed of the drum, relative location of the orifice to the drum, the viscosity of the melt at ejection, and the ejection pressure all impact the size and continuity of the wires. Many of these factors are not fully automated and lead to inconsistencies from repeated trials.

Wires were also produced using the Taylor liquid drawing technique. In this production method alloy pieces are insert into a thin Pyrex glass tube, which will be used to draw wires. The tube is subjected to vacuum and then filled with low pressure argon and sealed using a hydrogen flame. The alloy is then heated inside the tube over the oxyhydrogen flame. Once the glass softens and is able to be worked and the alloy is molten, the tube is pulled apart, leaving a glass capillary containing a microwire. Following heat treatment and quenching, the glass coating is removed by soaking the wires in a hydrofluoric acid solution.

2.2 Heat Treatment

Following casting, microwires were heat treated to stabilize the austenite phase and promote grain growth. Grain growth leads to the oligocrystalline, bamboo-like structure discussed earlier. This can substantially increases the mechanical properties of the microwires.

The wires were placed in quartz tubes, which were subjected to vacuum conditions before being filled with argon to prevent oxidation. Based on the phase diagrams of the specific composition of alloy, the wires were annealed at 800C-900C for 1-3 hours. The wires were water quenched to lock in the appropriate phase at room temperature.

2.3 SEM for Imaging and Composition Measurements

A scanning election microscope was used to create images and take measurements of microwires. The SEM allowed for measurements of diameters of wires and grain size, as well as identification of grain boundaries. In some cases martensitic plates were observed.

Energy dispersive x-ray spectroscopy was used to determine the composition of the wires. This was performed throughout the process of casting and heat-treating the wires.

2.4 Transition Temperatures

Differential scanning calorimetry was used to determine the transition temperatures of the microwires. The transition temperatures vary based on the composition of the wires and need to be known to inform the proper conditions for mechanical testing. Figure 2.2 shows a typical DSC curve for an as-cast and annealed Cu-Al-Ni wire. For the annealed wire the transition temperatures are approximately 110C and 140C for austenite start and finish temperatures, respectively, and 125C and 90C for the martensite start and finish temperatures, respectively.

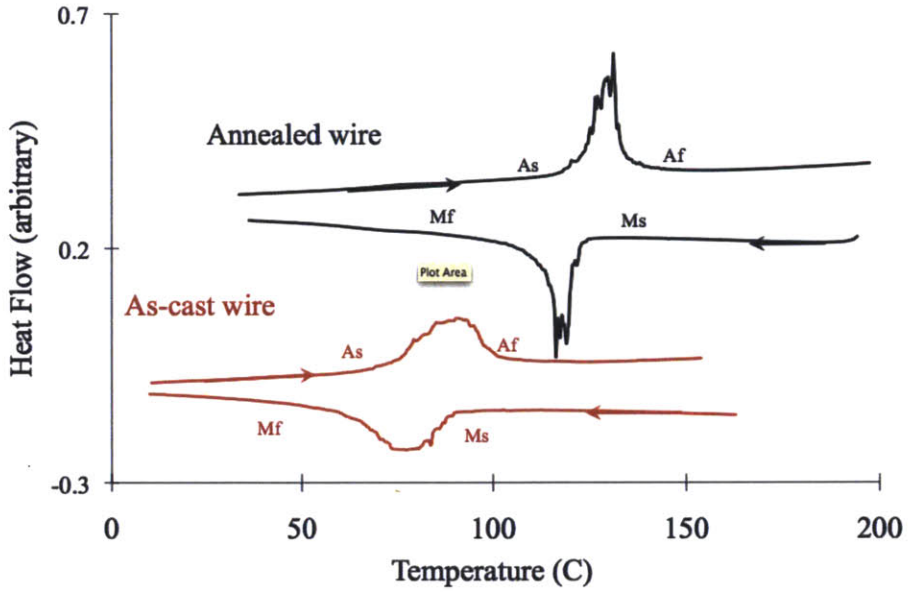

Figure 2.2. DSC curves for a Cu-Al-Ni wire. The upper, black curve is endothermic for the martensite to austenite transformation and the lower, black is exothermic for the austenite to martensite transformation for an annealed wire. The red curve represents the same transformations for an as-cast wire.

2.5 Electropolishing

Wires were electropolished in a 67% phosphoric acid solution for 7-15 minutes as recommended for copper alloys with significant aluminum content [21]. The electrodes were pure copper and the polishing voltage ranged from 2.0-3.0 volts. Surface defects, which are a likely place for cracks to develop, can be eliminated with electropolishing. Electropolishing is very useful for revealing grain size and grain boundaries in the microwires. Electropolishing is also effective at reducing the diameter of the wires, which can reduce stress concentrations and triple junctions.

Over polishing can also occur and is detrimental to the integrity of the wire. A non-uniform diameter will lead to different rates of attack and can lead to a necking-like effect where thin sections lead to failure. A lower polishing voltage can help diminish this drawback.

2.6 Mechanical testing

Microwires were tested for shape memory effect and superelastic properties using a dynamical mechanical analyzer with a closed furnace for temperature control. The ends of the wires were fastened into place using plastic mechanical grips, which were clamped tight. A high-resolution linear optical encoder within the furnace tracked the wire displacement to calculate strain. The gage length was measured to be 3-10 mm for different wires. The dimensions of the wire, after being measured using a SEM, were entered into the instrument in order to apply specific loads.

3. Results and Discussion

3.1 Wire casting

Microwires were successfully drawn using a melt spinner as detailed in Chapter 2.1. The different alloys led to the fabrication of many types of wires and the results were not consistent with repeated trials. Cu-Al-Ni was able to be drawn using crucibles with nozzles down to 100 um. Cu-Al-Mn-Ni was unable to be drawn at this nozzle size and had both successes and failures as the nozzle size was increased to 300 um.

The advantage of using the melt spinner over previously used methods is the length of the wires that can be drawn. This was shown with the drawing of wires greater than a meter in length. Many trials led to many pieces of wires around tens of centimeters in length, however some trials led to only small fragments of wires centimeters or less in length. Figure 3.1 shows the results of successive trials of Cu-Al-Ni. It can be clearly observed that MS-11 Cu-Al-Ni, shown on the left, produced longer and more wires than MS-9 Cu-Al-Ni, shown on the right. The width of MS-11 was measured to be greater than that of MS-9, at 150-160 um versus 75-100 um. Additionally, MS-9 yielded many fragments of wires only millimeters in length. These trials had very similar operating condition, but the human element controlling the placement of the nozzle relative to the drum, current through the induction coil, and the timing of the ejection led to different outcomes.

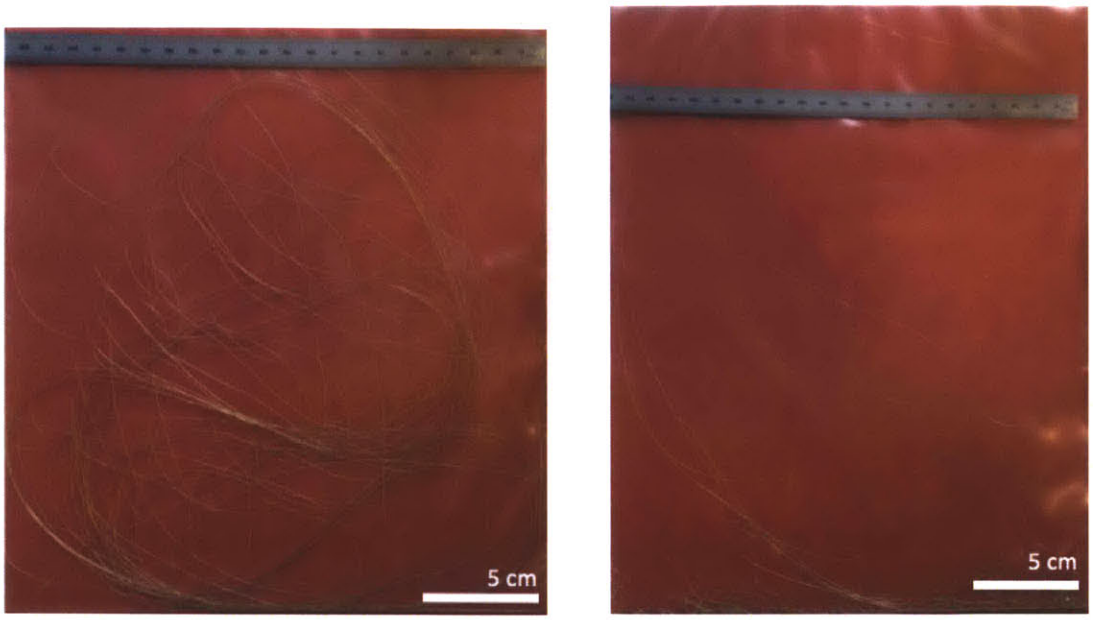

(a) (b)

Figure 3.1. (a) Microwires obtained from trial MS-11 Cu-Al-Ni and (b) MS-9 Cu-Al-Ni.

The wires cast using the melt spinner were rectangular in cross section, not circular. This was easily observed while handling the wires. This was not the case for the wires drawn using the Taylor method, which were circular in cross section.

3.2 Compositions

The composition of some alloys changed during the processes of casting the alloy into microwires and heat treatment. Metal powders were mixed for compositions within the aluminum range described by the phase diagrams. However, the aluminum content increased considerably for some Cu-Al-Ni wires and in one case nickel content also rose significantly.

Table 3.1 shows the changes in composition of MS-9 at different stages in the process and after 3 different heat treatment methods. A decreasing trend of the amount of copper and nickel is observed, while the amount of aluminum increases with treatment.

MS-9	Wire Composition (wt%)		
	Cu	Al	Ni
Alloy	80.0	13.9	6.2
Wire – as cast	78.3	15.4	6.3
Wire – HT 850C – 1hr	77.0	16.7	6.3
Wire – HT 870C – 2.5hr	75.8	18.7	5.4
Wire – HT 870C – 2.5hr, 850C – 1hr	74.5	20.2	5.3

Table 3.1. Composition of a MS-9 Cu-Al-Ni wire throughout fabrication and post processing.

Considerable losses of copper are noticed after casting and heat treatment. The resulting wires are not in the range for shape memory properties. Copper is being lost due to oxidation, non-homogeneity of the mixture, or due to a zone refining effect as different parts of the alloy are melted and solidified during wire casting.

A MS-6 wire shows nickel content at 24% weight, approximately 6 times higher than the original mixed composition. This wire also has very high aluminum content, 39% weight. The original intended composition of this wire was 79.96%Cu-12.43%Al-4.45%Mn-3.16%Ni.

However, in general the Cu-Al-Mn-Ni wires showed more consistent composition. An EDS plot of a MS-3 Cu-Al-Mn-Ni wire shows weight percents of 80.6%Cu-12.3%Al-3.9%Mn-3.2%Ni in Figure 3.2

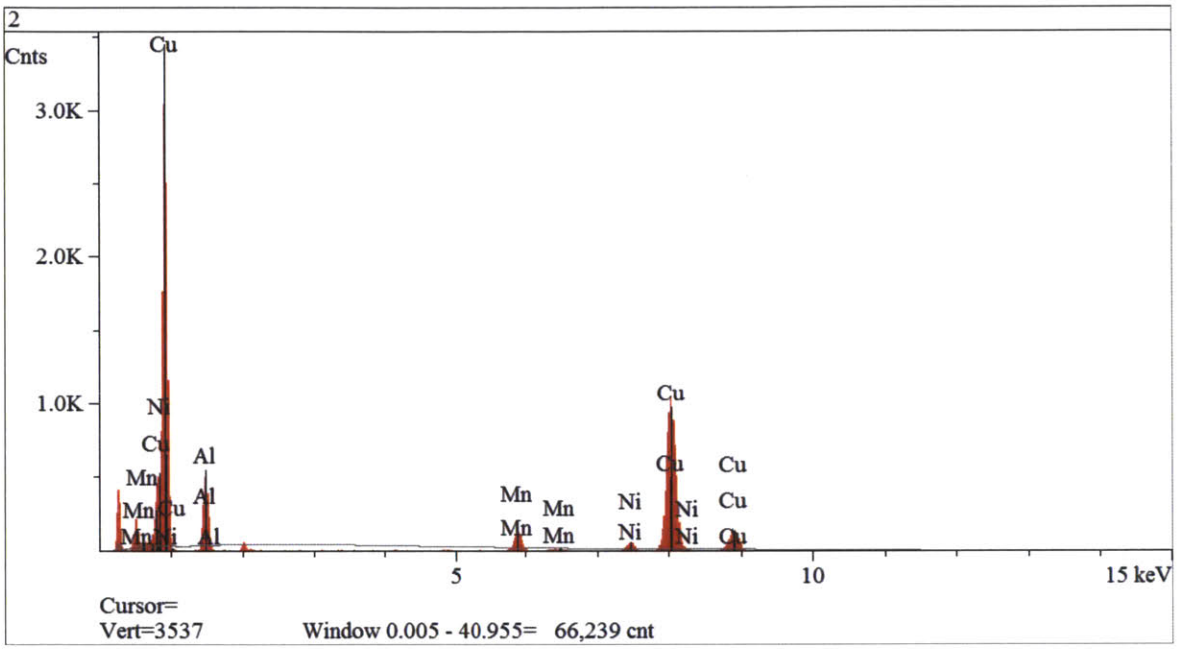

Figure 3.2. An EDS plot of an MS-3 Cu-Al-Mn-Ni wire heat treated at 800C for 3 hours.

Wires drawn using the Taylor method also showed more consistent compositions. The absence of the melt spinner for production lead to no loss of copper in the drawing process and the glass coating provided another layer of protection during annealing. The wires produced with the Taylor method had a composition of 79.0%Cu-15.1%Al-5.9%Ni, very close to the original prepared alloy. However, non-homogeneities in composition were observed over all wires. Even in wires produced with the Taylor method, while the average composition was very

clearly near the alloy composition, aluminum rich and copper poor sections were encountered. This non-homogeneity could compromise mechanical performance.

Alloys were also prepared with intentionally high copper weight percentages, expecting to lose copper as the alloys and wires are processed. Aluminum content for these alloys ranged from 8-10% weight. These alloys were ejected at higher temperatures than the other alloys, near 1400C as opposed to near 1200C. However, continuous wires were unable to be cast using these compositions.

3.3 Electropolishing and Imaging

Wires were electropolished to improve the quality of the surface of the wires. This process helps to alleviate sources of stress concentrators and reduce wire diameter to eliminate triple junctions. A polished surface also allowed for grain boundaries to be more easily identified.

Only a few minutes were necessary to smooth the surface of the wires with more time decreasing wire diameter until over polishing occurs. Figure 3.3 shows a before and after pictures for a Cu-Al-Mn-Ni wire. The before image shows a rough surface of the annealed wire with an average width of 210 um. After 4 minutes of electropolishing at 3.0 V and 0.12 A the surface is smooth and the average width has decreased to 180 um. Increasing the electropolishing time to 25 minutes results in an even smoother surface. In this case the width of the wire has become more uniform in this section. The average width has decreased to 110 um, close to the size where size effects begin to improve the performance of microwires [10].

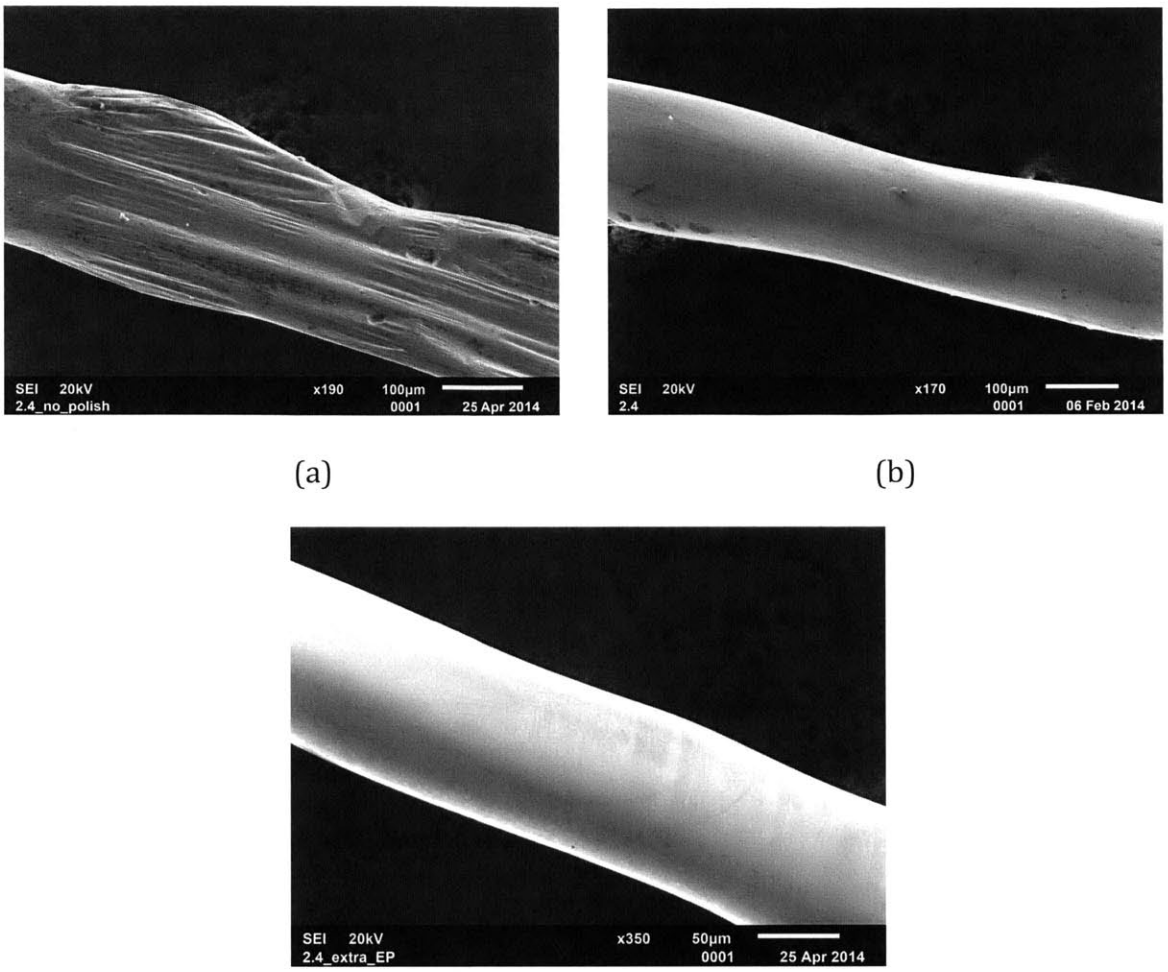

Figure 3.3. (a) Before and (b) after images of a Cu-Al-Mn-Ni wire. (c) Shows the diameter decreasing further with more electropolishing.

As cast wires could be as large as 300 um, which were very likely to be riddled with performance impairing triple junctions. Figure 3.4 shows a montage of a section of a wire that was electropolished for 20 minutes at 3 V and 0.13 A. The grain boundaries can be easily seen and triple junctions are identified near the center and right side of the images. Additional electropolishing decreased the size of these triple junctions. Even further electropolishing could eliminate triple junctions completely leaving only the desired bamboo structure, but in this case the other areas of the wire failed before this could occur.

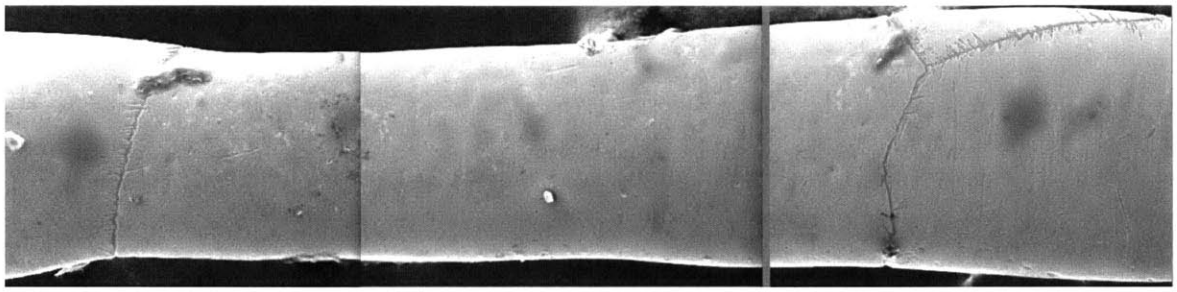

(a)

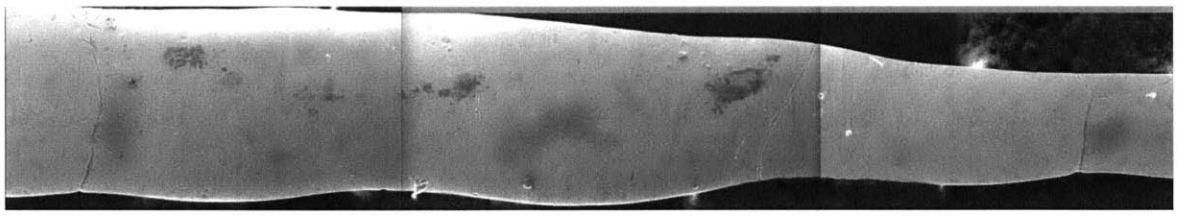

(b)

Figure 3.4. A montage of SEM images of grains in a Cu-Al-Mn-Ni wire. (a) Is the left side and (b) the right side. The width at the right end in (b) is 110 um and the average width of the rest of the wire is 175-215 um.

Electropolishing rates were determined for MS-3 Cu-Al-Mn-Ni microwires. Figure 3.5 shows a plot of mass loss per starting surface area vs. time. The starting wire cross section dimensions was approximately 325 um by 100 um and exposed lengths of 15-18mm. The plot shows a rate of mass loss to be 0.011 $\frac{g}{mm^2 * \min}$. Assuming equal mass loss along the length of the microwire, this rate can be used to determine the time required to reach a specified final wire size. As surface area decreases, current density and the rate of material loss increases this assumption does not hold, which can lead to over polishing. If a wire does not have a consistent diameter to begin with, thin sections are attacked more rapidly than other sections. This can lead to a weak spot in the wire under mechanical testing or the wire breaking in the polishing solution. This occurred during attempted testing of electropolishing rates for thinner wires.

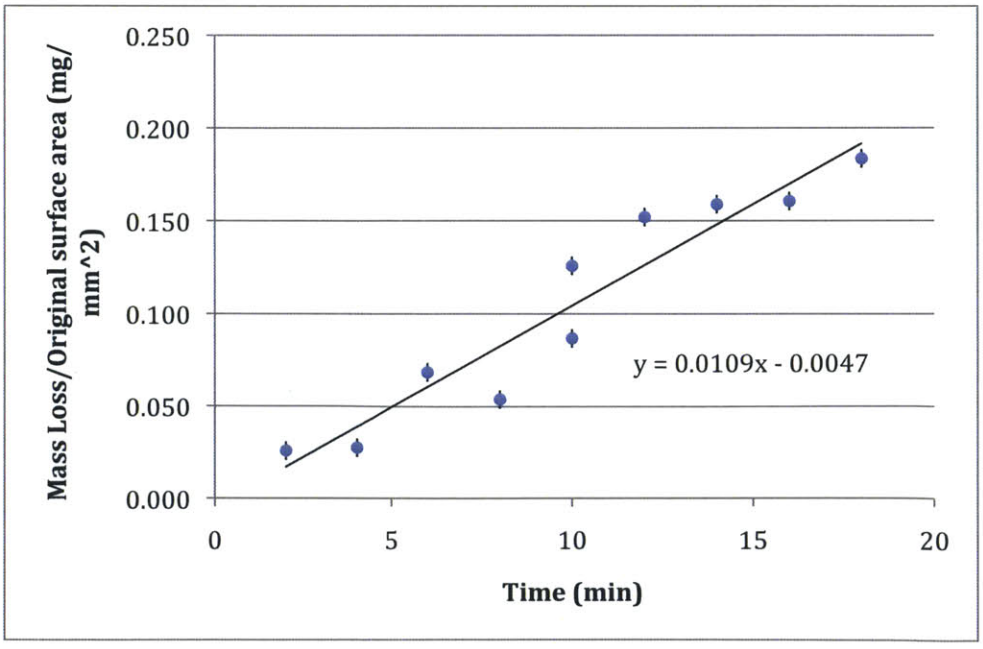

Figure 3.5. Electropolishing rates for MS-3 Cu-Al-Mn-Ni microwires.

Figure 3.6 shows a wire drawn using the Taylor method. The wire is shown with the glass coating still around the wire, except for a section in the middle where the unpolished wire is exposed. The wire shows a very uniform diameter of 97 um.

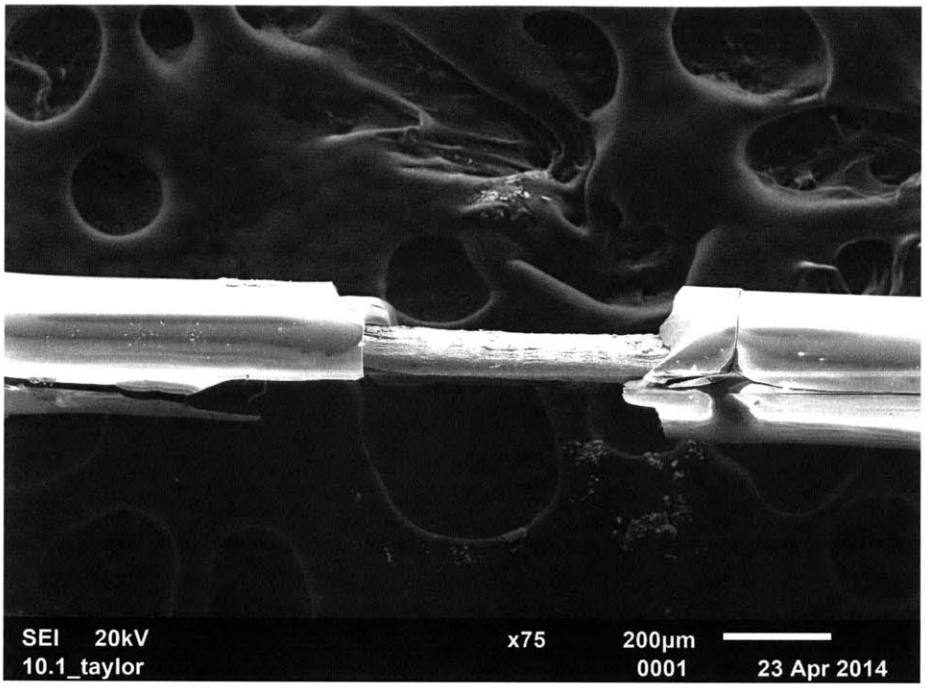

Figure 3.6. SEM image of a wire produced using the Taylor drawing method. The fractured glass capillary is seen around the wire.

3.4 Mechanical Testing

Composition issues led to poor mechanical performance of the wires. Many wires with correct, or within range for shape memory properties also did not perform well, possibly due to the increased size of these wires. Larger cross sections are more likely to contain detrimental triple junctions. Several wires were tested under shape memory effect and pseudoelastic conditions. The

transformation temperatures for Cu-based alloys are significantly higher than Ni-Ti based systems, which transition near room temperature.

Figure 3.7 shows shape memory hysteresis for a MS-3 Cu-Al-Mn-Ni wire, which was heat treated at 800C for 3 hours. There are clear transition temperatures, which are seen to increase with applied stress. However, the strains are observed to be around 1 percent and not fully recoverable, which is not sufficient for shape memory applications. The cross section of the wire measured 200 um x 105 um.

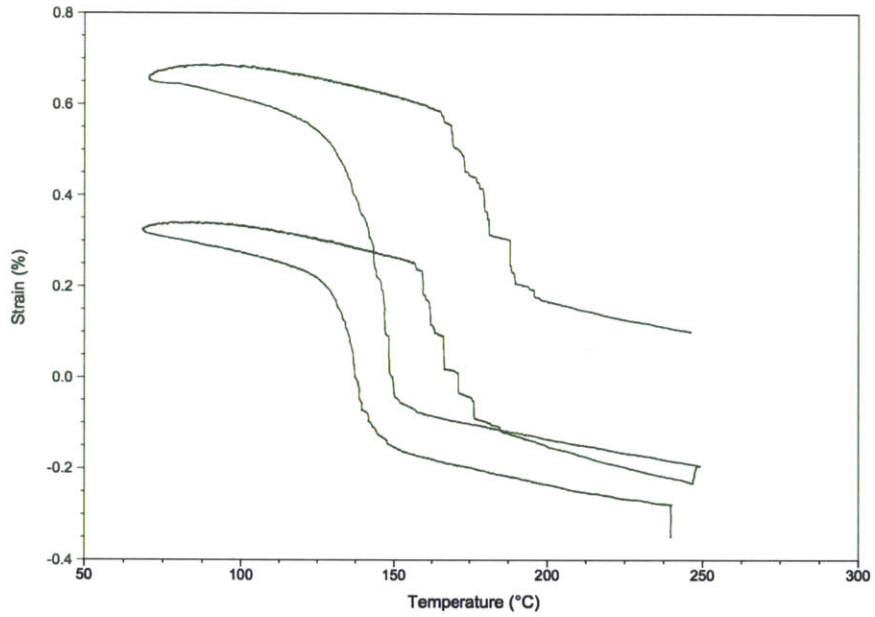

Figure 3.7. Shape memory hysteresis for a Cu-Al-Mn-Ni wire. The applied stresses were 20 MPa and 40 MPa.

Figure 3.8 shows shape memory hysteresis for a MS-11 wire as cast, with no heat treatment. This thermal cycle shows improved strain, greater than 2.5%, but no clear transition temperatures. This is likely due to the wire being highly polycrystalline as grains were not given time to grow through heat treatment. The wire cross section measured 150 um x 70 um.

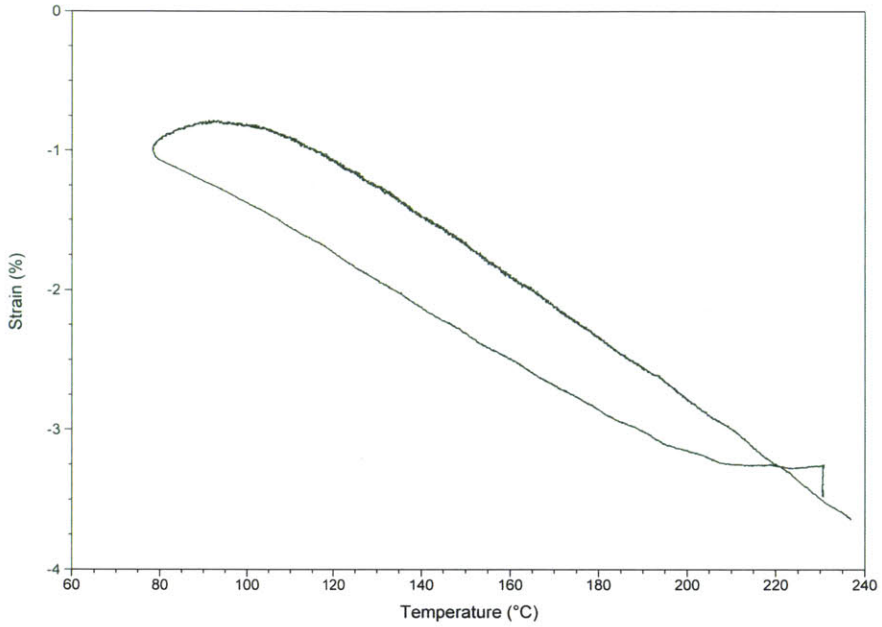

Figure 3.8. Shape memory hysteresis for an as cast MS-11 CuAlNi wire. The applied stress was 20 MPa.

Despite correct or near correct compositions for many wires including the MS-3 Cu-Al-Mn-Ni, MS-11 Cu-Al-Ni, and the Taylor method Cu-Al-Ni wires, adequate shape memory properties were not observed. In addition to size and triple junction's potential impact on performance, non-homogeneity or poor quenching may have contributed to poor performance. If not enough of the microwire had the proper β-phase, shape memory properties would not be observed.

4. Conclusions

Cu-based shape memory alloys remain a promising alternative to expensive Ni-Ti alloys. With a higher working temperature than Ni-Ti alloys, Cu-based SMAs can reach a variety of new applications.

This work showed that the long length scales of Cu-Al-Ni and Cu-Al-Mn-Ni microwires needed for the creation of complex structures can be successfully achieved with a melt spinner. Continuous wires greater than a meter in length were produced in addition to numerous wires of shorter, but still useful length. The melt spinner shows promise as an alternative to hand or automated wire fabrication using the Taylor liquid drawing technique. Composition consistency from alloy to annealed microwire and uniform shape remain issues.

SEM imaging revealed the melt spinner is able to produce oligocrystalline wires on the length scale for improved shape memory property performance. Electropolishing was found to successfully improve surface quality and further reduce wire size to eliminate triple junctions.

5. Future Work

This research has identified several areas that require more detailed investigations in order to further understand the potential applications of Cu-based shape memory alloys.

A more robust method for wire fabrication is needed. An in depth study on the melt spinner would help to enable future success. The melt spinner needs to have more predictable and repeatable results. The basic properties of the wires (size, shape, composition) need to be produced consistently before this work proceeds.

The composition changes from alloy casting to wire casting and annealing should also be studied. Composition differences impact the heat treatment temperatures needed to stabilize the β-phase for shape memory properties. Deviations from target composition or non-homogeneities significantly decrease performance of the wires and must to be corrected.

Finally, the investigation of the use of microwires in complex structures, such as braided cables and fabrics, is a very exciting opportunity for future work. Potential applications are high in this area and successful production of long wires with improved shape memory properties could make this an exciting area of research.

References

[1] Olander, A. (1932) J. Amer. Chem. Soc. 54: 3819
[2] Chang LC, Read TA. T Am I Min Met Eng 1951;191:47.
[3] Sato, A. et al. *Orientation and composition dependencies of shape memory effect in Fe-Mn-Si alloys.* Acta Metallurgica, Vol 32 Issue 4 1984
[4] Otsuka K, Ren X. Prog Mater Sci 2005;50:511.
[5] Otsuka K, Sakamoto H, Shimizu K. Acta Metall Mater 1979;27:585.
[6] Wu, Ming H and Schetky, L. Mc.D.. *Industrial Applications for Shape Memory Alloys*, Proceedings of the International Conference on Shape Memory and Superelastic Technologies, Pacific Grove, CA, p.171-182 (2000).
[7] MIT 3.022 Lecture, Cima, Spring 2012
[8] Hane, Kevin H. *Microstructures in Thermoelastic Martensitic Transformations.* Mechanics of Materials
[9] Ueland, S.M. *Grain Constraint and Size Effects in Shape Memory Alloy Microwires* Massachusetts Institute of Technology, 2013
[10] Chen Y., Schuh C. *Size effects in shape memory alloy microwires.* Acta Materialia 59 (2011) 537-553.
[11] Miura, S. and Maeda, S. *Pseudoelastic and Shape Memory Phenomena related to Stress-Induced Martensite in Cu-15 at % Sn Alloy.* Scripta Metallurgica, Vol. 9, pp. 675-680, 1975.
[12] We, S; Wayman C (1987). "Martensitic transformations and the shape-memory effect in Ti50Ni10Au40 and Ti50Au50 alloys". *Metallography* **20** (3):359
[13] Buehler, W.J. et al. *Effect of Low Temperature Phase Changes on the Mechanical Properties of Alloys near Composition NiTi.* Journal of Applied Physics **34**, 1475 (1963).
[14] Wang, F.E. et al. *Crystal Structure and a Unique "Martensitic" Transition of TiNi.* Journal of Applied Physics **36**, 3232 (1965).
[15] NDC "Nitinol Facts"
[16] Wilkes, K. E.; Liaw, P.K. (2000), "*The fatigue behavior of shape memory alloys*" JOM **52** (10): 45
[17] Cederstom J., Van Humbeeck J. (1995). "*Relationship between Shape Memory Material Properties and Applications*". J Physics IV **5**: C2-325
[18] calibamboo.com/bamboopoles.html
[19] Dunne, D.P., Kennon, N.F. *Ageing of Copper-based Shape Memory Alloys.* Metals Forum, Volume 4, Issue 3, Pages 176-183
[20] Phoenix Scientific Industries Ltd.
[21] Davis, Joseph R. Copper and Copper Alloys ASM International, 2001